

The Self-Similarity of Shear-Dominated Viscous Stirring

Benjamin F. Collins, Hilke E. Schlichting, and Re'em Sari

California Institute of Technology, MC 130-33, Pasadena, CA 91125

bfc@tapir.caltech.edu

ABSTRACT

We examine the growth of eccentricities of a population of particles with initially circular orbits around a central massive body. Successive encounters between pairs of particles increase the eccentricities in the disk on average. As long as the epicyclic motions of the particles are small compared to the shearing motion between Keplerian orbits, there is no preferred scale for the eccentricities. The simplification due to this self-similarity allows us to find an analytic form for the distribution function; full numerical integrations of a disk with 200 planetesimals verify our analytical self-similar distribution. The shape of this non-equilibrium profile is identical to the equilibrium profile of a shear-dominated population whose mutual excitations are balanced by dynamical friction or Epstein gas drag.

Subject headings: planets and satellites: formation — solar system: formation

1. INTRODUCTION

Modern computational power allows the simultaneous integration of the orbits of increasingly numerous particles. Much of the planet formation process, however, involves particle numbers that exceed the limits of computational efficiency. This limitation is often circumvented with a statistical approach. By monitoring the gravitational interactions of the particles in a time-averaged sense, various properties of the particle population can be calculated without a full N -body simulation.

Collins & Sari (2006), hereafter Paper I, motivate a Boltzmann equation to describe the evolution of the eccentricity distribution of an ensemble of particles in which the relative motion between any two interacting particles is dominated by the shearing motion of close circular orbits. Such a regime of orbital eccentricities is called shear-dominated. The solution of their equation provides a simple analytic expression for the equilibrium eccentricity distribution that results when dynamical friction can balance the mutual interactions of the particles; the analytic expression matches results from numerical simulations remarkably well.

In this letter we derive analytically the non-equilibrium distribution function of interacting shear-dominated particles in the absence of dynamical friction. §2 reviews the construction of the

Boltzmann equation. In §3, we show that the distribution function behaves self-similarly, and the shape of the non-equilibrium distribution function is identical to the equilibrium distribution of Paper I. §4 corroborates this result with numerical simulations. Conclusions follow in §5.

2. THE TIME-DEPENDENT BOLTZMANN EQUATION

We consider a disk of particles on initially circular orbits around a massive central body. We write their surface mass density σ and the mass of a single body m . The number density, σ/m is sufficiently low that three-body encounters are very rare, therefore the orbital evolution of each body is well described as a sequence of pair-wise encounters.

The change in eccentricity due to one such encounter can be calculated analytically. For completeness, we summarize the derivation presented in Paper I. Let one particle, with a semi-major axis a , encounter another with semi-major axis $a + b$. In the limit of $b \ll a$, the relative orbital frequency between the pair is $\Omega_r = (3/2)\Omega b/a$, where Ω is the Keplerian orbital frequency for a semi-major axis a . If in addition $b \gg R_H \approx (m/M_\odot)^{1/3}a$, the change in eccentricity from one encounter is $e_k = A_k(m/M_\odot)(b/a)^{-2}$, where $A_k \approx 6.67$ collects the order-unity coefficients (Goldreich & Tremaine 1978; Petit & Henon 1986).

The eccentricity is not the only Keplerian element that characterizes the non-circular motion of a particle; the longitude of periapse specifies the relative orientation of a particle’s epicycle. The particles may also follow orbits that do not lie in the disk. However, shear-dominated viscous stirring excites inclinations at a rate that is always slower than the excitation of eccentricities (Wetherill & Stewart 1993; Goldreich et al. 2004; Rafikov 2003). The perpendicular velocities are, in this case, always negligible compared to the epicyclic motion in the disk plane.

The magnitude of an orbit’s eccentricity and the longitude of periapse together specify a two-dimensional parameter space. We describe the two-dimensional variable with a vector, $\mathbf{e} = \{e \cos \omega, e \sin \omega\}$. The distribution function is a function of this vector and time, $f(\mathbf{e}, t)$. That the changes in \mathbf{e} due to encounters do not depend on the longitude of periapse already shows that the distribution function must be axisymmetric, or $f(\mathbf{e}, t) = f(e, t)$. Then the number of bodies per unit logarithmic interval around e is given by $2\pi e^2 f(e, t)$.

We characterize the eccentricity growth with a differential rate, $p(\mathbf{e}_k)d^2\mathbf{e}_k$, that the eccentricity vector of a particle will be changed by an amount \mathbf{e}_k . Since the change in eccentricity experienced by a pair of bodies, when treated as a vector quantity, is independent of the initial eccentricity vector of each body, this function is also axisymmetric and only depends on the magnitude of the change of eccentricity, e_k .

The excitation rate depends on the surface mass density of particles in the disk, σ , the mass of a single body, m , the mass of the central star, M_\odot , the cross-section at which a particle experiences encounters of a strength e_k , and the relative speed of those encounters. The impact parameter at

which a particle receives an eccentricity e_k scales as $b \sim e_k^{-1/2}$. If the eccentricities are small, the speed at which one particle encounters the others is set only by the shearing of their two orbits, which is proportional to b . Then, as shown in Paper I,

$$2\pi p(e_k)e_k de_k = 3\frac{\sigma}{m}\Omega b(e_k)db(e_k). \quad (1)$$

After simplification, we find

$$p(e_k) = \frac{A_k}{4\pi} \frac{\sigma a^2}{M_\odot} \frac{1}{e_k^3} \Omega. \quad (2)$$

An integral over every e_k dictates the rate of change of the number of bodies with a given eccentricity, e :

$$\frac{\partial f(e, t)}{\partial t} = \int \int p(|\mathbf{e} - \mathbf{e}_n|) [f(e_n, t) - f(e, t)] d^2 \mathbf{e}_n. \quad (3)$$

Note that this equation implicitly conserves the total particle number, $\int \int f(e, t) d^2 \mathbf{e} = 1$. This can be shown by integrating both sides with respect to \mathbf{e} .

3. THE SELF-SIMILAR DISTRIBUTION

Without a specific eccentricity scale to dictate the evolution of $f(e, t)$, we expect a solution of the form,

$$f(e, t) = F(t)g(e/e_c(t)). \quad (4)$$

Replacing $f(e, t)$ in equation 3 with equation 4, we find,

$$\frac{1}{F(t)} \frac{\partial F(t)}{\partial t} e_c(t)g(x) - x \frac{\partial g(x)}{\partial x} \dot{e}_c(t) = \int \int p(|\mathbf{x} - \mathbf{x}_n|) [g(x_n) - g(x)] d^2 \mathbf{x}_n, \quad (5)$$

where $\mathbf{x} = \mathbf{e}/e_c(t)$. The additional constraint that equation 3 conserves particle number implies $F(t)e_c(t)^2$ is constant. This relationship simplifies the left side of equation 5 such that the only possible time-dependence of each term is contained in $\dot{e}_c(t)$. The right-hand side, however, is independent of time. Therefore $\dot{e}_c(t)$ must be constant. Then,

$$e_c(t) = C_e t \text{ and } F(t) = (C_e t)^{-2}. \quad (6)$$

The overall normalization of $F(t)$ is arbitrary, as it can be absorbed into $g(x)$. Our choice of $F(t)$ requires $\int \int g(x) d^2 \mathbf{x} = 1$ to ensure that $\int \int f(e, t) d^2 \mathbf{e} = 1$ for all t . Physically, the typical eccentricity, $e_c(t)$, is set by the eccentricity change that occurs once per particle per time t , or, $e_c(t)^2 p(e_c(t)) t \sim 1$. This argument sets $e_c(t)$ only up to a constant coefficient; for simplicity we choose the coefficients such that $e_c(t) = (A_k/2)(\sigma a^2/M_\odot)\Omega t$. Then, the profile shape, $g(x)$, is specified by the integro-differential equation

$$2g(x) + x \frac{\partial g(x)}{\partial x} + \frac{1}{2\pi} \int \int \frac{g(x_n) - g(x)}{|\mathbf{x}_n - \mathbf{x}|^3} d^2 \mathbf{x}_n = 0, \quad (7)$$

Equation 7 is identical to equation 17 of Paper I. A detailed description of the equation and a proof of its solution can be found in that paper. For reference, the solution is

$$g(x) = \frac{1}{2\pi} (1 + x^2)^{-3/2}, \quad (8)$$

4. NUMERICAL SIMULATIONS

The non-equilibrium distribution function of eccentricities in the regime discussed above can be measured directly from a full numerical simulation of the disk. We use a custom N-body integrator that evolves the changes in the two-body constants of motion of each particle around the central mass. These constants are chosen to vary slowly with small perturbations. Solving Kepler's equation for each body translates each time-step into a change in orbital phase. The constants of motion are then integrated by a fourth-order Runge-Kutta routine with adaptive time-steps (Press et al. 1992).

For this study we follow a disk of two-hundred equal mass bodies, with $m = 5 \times 10^{-9} M_\odot$, on initially circular orbits with randomly determined phases and semi-major axes within a small annulus of width $\Delta a = 0.8a$. To avoid possible artifacts from the edge of the simulation, we only measure the eccentricities of the bodies in the central third of the disk. A histogram of those eccentricities shows the number of bodies with each eccentricity, $e \, dN/de$. To increase the signal to noise ratio of the histogram at each time, we add the results of one hundred simulations with randomly generated initial semi-major axes and orbital phases.

Figure 1 shows the eccentricity distributions measured after three and ten orbits. The horizontal error bars indicate the width of each bin, and the vertical error bars are determined assuming that each bin is Poisson distributed. The analytic distribution function derived in §3 for each time is also plotted, as a solid line. The measured distributions agree remarkably with the analytic result.

To emphasize the self-similarity of the distribution shape, we scale the eccentricities measured at each time by the characteristic eccentricity at that time ($e_c(t)$, given by equation 6) and plot the

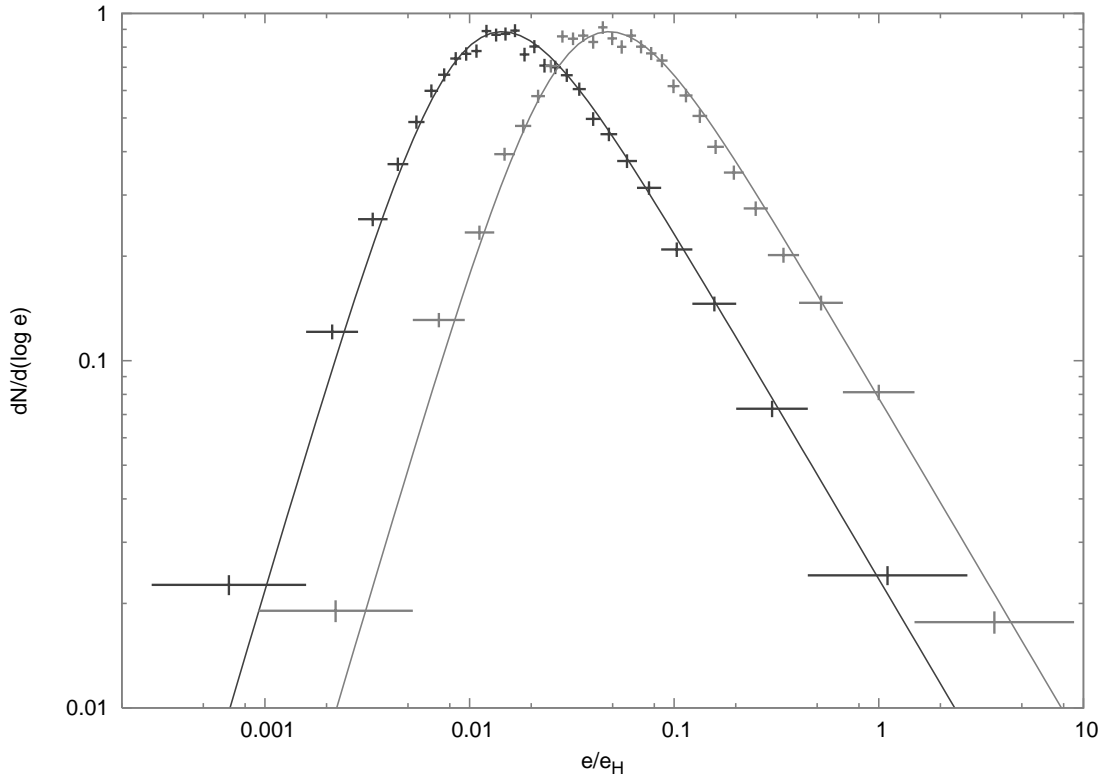


Fig. 1.— Eccentricity distributions of a shear-dominated disk of 200 particles each with a mass $m = 5 \times 10^{-9} M_{\odot}$ after three (black line) and ten (gray line) orbits. The average surface mass density of the simulated annulus is $3 \times 10^{-3} \text{g cm}^{-2}$. The vertical error bars are estimated by assuming each bin obeys Poisson statistics. The width of each bin has been chosen such that each bin contains a similar number of particles.

shapes added together. Figure 2 shows that the resulting distribution shape matches the analytic form of $g(x)$ very well.

5. DISCUSSION

We have written a time-dependent Boltzmann equation that describes the eccentricity distribution function of a population of orbiting particles under the influence of their mutual excitations in the shear-dominated regime. Reasoning that the distribution function of eccentricities should behave self-similarly, that is, retain a constant profile while its normalization and scaling depend on time, we have reduced the Boltzmann equation to a form that has already been shown to have an analytic solution. Numerical experiments confirm the self-similarity and the analytic solution.

Although we have only considered disks of a single particle size, the formalism above applies trivially to disks with mass distributions. In fact, the characteristic eccentricity, equation 6, depends only on the total surface mass density of the disk. As long as bodies of every part of the mass spectrum are in the shear-dominated regime, the eccentricities of all bodies are drawn from the same distribution. This is a consequence of the fact that gravitational acceleration is mass-independent. In contrast, the dynamical friction of Paper I depends on the size of each particle. The equilibrium distributions in that case do differ for each mass group.

Since $e_c(t)$ is an increasing function of time, the condition of shear-dominated dynamics will be violated eventually. While the disk is shear-dominated however, most of the disk bodies have eccentricities of about $e_c(t)$. The mean eccentricity, $\int \int e f(e, t) d^2 \mathbf{e}$, is formally infinite; in reality the mean depends logarithmically on the maximum eccentricity achievable from one interaction. Higher moments of the distribution, such as $\langle e^2 \rangle$, are dominated by the bodies with the maximum eccentricity. The random kinetic energy of the disk bodies, for example, is then set by the few bodies with the highest eccentricities regardless of the value of $e_c(t)$.

That the shape of the distribution function is identical to the distribution function of Paper I is ultimately not surprising. In both scenarios the bodies in question excite their orbital parameters via the same shear-dominated viscous stirring mechanism. If dynamical friction is acting on these bodies, their eccentricities decrease with time proportionally to their magnitude. An equilibrium between excitations and this damping produces a characteristic eccentricity around which the eccentricities of all bodies are distributed. Without an agent of dynamical friction, the typical eccentricity of a body in the disk, $e_{\text{typical}} \sim e_c(t)$, grows with time. However, the ratio of the eccentricity of a particle that has not interacted recently, e , to that typical eccentricity shrinks proportionally to itself:

$$\dot{x} \equiv \frac{d}{dt} \left(\frac{e}{e_c(t)} \right) \sim -x. \quad (9)$$

This is formally equivalent to the damping provided by the dynamical friction of Paper I.

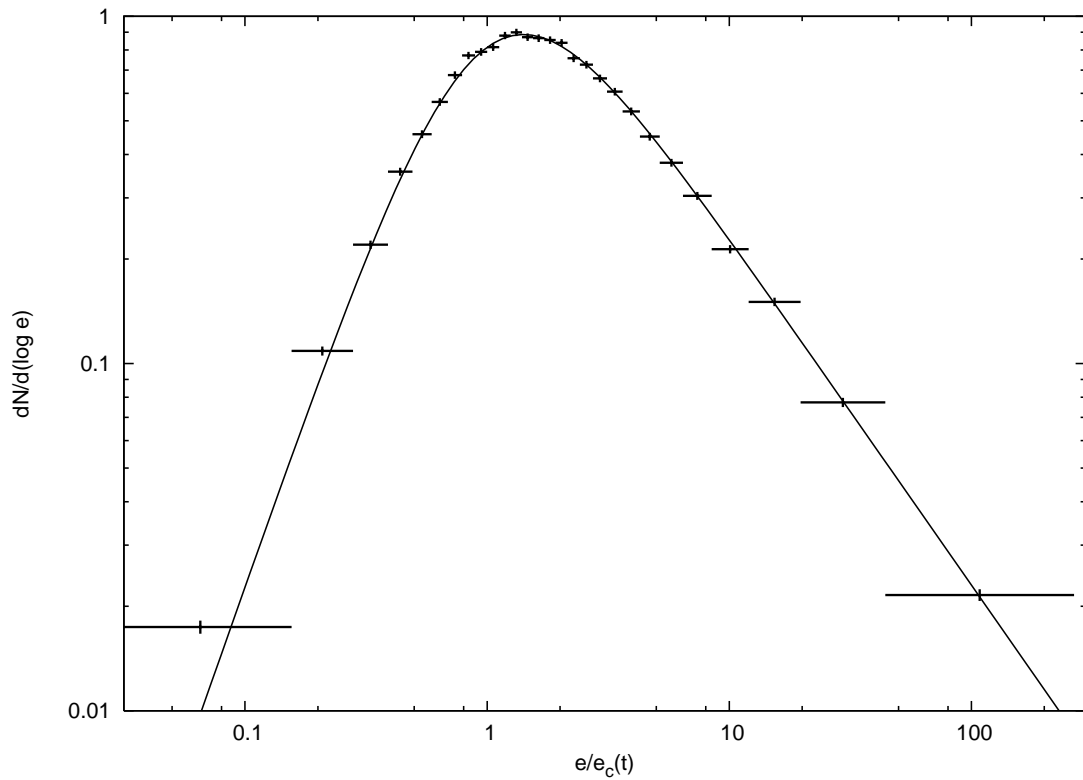


Fig. 2.— The eccentricity distribution of the same numerical simulation of Figure 1. Here, the distribution after one, three, and ten orbits, scaled by the characteristic eccentricity at that time are added together. The profile shape is very well described by equation 8, plotted as a solid line. The error bars are chosen in the same way as Figure 1.

REFERENCES

- Collins, B. F., & Sari, R. 2006, AJ
- Goldreich, P., Lithwick, Y., & Sari, R. 2004, ARA&A, 42, 549
- Goldreich, P., & Tremaine, S. D. 1978, Icarus, 34, 227
- Petit, J.-M., & Henon, M. 1986, Icarus, 66, 536
- Press, W. H., Teukolsky, S. A., Vetterling, W. T., & Flannery, B. P. 1992, Numerical recipes in C. The art of scientific computing (Cambridge: University Press, —c1992, 2nd ed.)
- Rafikov, R. R. 2003, AJ, 125, 942
- Wetherill, G. W., & Stewart, G. R. 1993, Icarus, 106, 190